Available online at www.sciencedirect.com
ScienceDirect
Journal of Molecular Catalysis A: Chemical 279 (2008) 77–81
JOURNAL OF MOLECULAR CATALYSIS A: CHEMICAL
www.elsevier.com/locate/molcata

The preparation, characterization, and photocatalytic activities of Ce-TiO_2/SiO_2

Yue-hua Xu *, Zhuo-xian Zeng

Department of Applied Chemistry, College of Science, South China Agricultural University, Guangzhou 510642, China

Received 19 August 2007; accepted 15 September 2007
Available online 21 September 2007

Abstract

A series of Ce-TiO_2/SiO_2 (Ce-TiO_2 coatings on SiO_2) were prepared by the sol–gel process and characterized by TG–DTA, XRD, SEM, XPS and DRS. The photocatalytic activities of Ce-TiO_2/SiO_2 for the oxidation of formaldehyde irradiated by 250 W high-pressure mercury lamp were investigated. According to XPS investigation, the Ti element mainly existed as the chemical state of Ti^{4+}, and Ce is present mainly in the +4 oxidation state and a little in the +3 oxidation state. The effect of cerium content on the photocatalytic activities was studied, and the result reveals that 0.10%Ce-TiO_2/SiO_2 exhibits highest photoactivity. The light absorption of Ce-TiO_2/SiO_2 increases with increasing cerium content, and cerium doping causes absorption spectra of Ce-TiO_2/SiO_2 to shift to the visible region. The high photocatalytic activity of Ce-TiO_2/SiO_2 can be explained by the effective separation of photogenerated electron–hole pairs, which are trapped by Ce^{4+} and hydroxyl groups balancing the positive charge generated by the incorporation of Si in a Ti matrix, respectively.

Keywords: Formaldehyde; Photocatalytic degradation; Ce-TiO_2/SiO_2; Cerium doping; Commercial silica

1. Introduction

Recent investigations have showed that semiconductor powders, such as TiO_2 that is well known for its advantage as a photocatalyst, suspended in solution can be utilized for photocatalytic oxidation of organic pollutants. However, practical applications of photocatalysis are limited because of problems of low photoefficiency, separation of fine particles of TiO_2 used after the treatment process and the recycling of the photocatalyst [1]. Many techniques [2–4] were proposed for the immobilization of TiO_2 on solid supports to eliminate these problems. In conjunction with SiO_2 or doping rare-earth element [5–6] have been extensively studied and found that the photocatalytic activity of TiO_2 increased. Xie et al. [7] reported the visible-light induced photodegradation of X-3B by cerium modified titania sol and nanocrystallites. Liu et al. [8] showed that the CeO_{2-y}-TiO_2 powders could apparently shift the UV-absorption band of TiO_2 toward visible range, and the doping of 5 wt% CeO_{2-y} gave the maximum absorption in the range of 380–460 nm. Yan et al. [9] found that TiO_2/SiO_2 could be used repeatedly and showed a higher photocatalytic decomposition rate for dichlorvos than TiO_2. In the present work, a series of Ce-TiO_2/SiO_2 (Ce-TiO_2 coatings on SiO_2) were prepared by the sol–gel method with precursors of ammonium cerium(IV) nitrate and tetra-*n*-butyl titanate. In order to examine the mechanism, we characterized Ce-TiO_2/SiO_2 with TG–DTA, XRD, SEM, XPS, and DRS. In this study the photocatalytic activity of Ce-TiO_2/SiO_2 for the degradation of formaldehyde was also investigated.

2. Experimental

2.1. Photocatalyst preparation

A series of Ce-TiO_2/SiO_2 with Ce-doped content in the range of 0.01–1.00 mol% were prepared by sol–gel method. The preparation was carried out as follows: absolute alcohol and diethanolamine were added to $Ti(O\text{-}Bu)_4$, and then redistilled water was added dropwise under stirring. The required ammonium ceric nitrate content was then dissolved into the above solution under continuous stirring for 1 h, and then polyethylene glycol was dissolved to obtain sol.

* Corresponding author. Tel.: +86 20 85281989.
E-mail address: xuyuehua@scau.edu.cn (Y.-h. Xu).

1381-1169/$ – see front matter © 2007 Published by Elsevier B.V.
doi:10.1016/j.molcata.2007.09.016

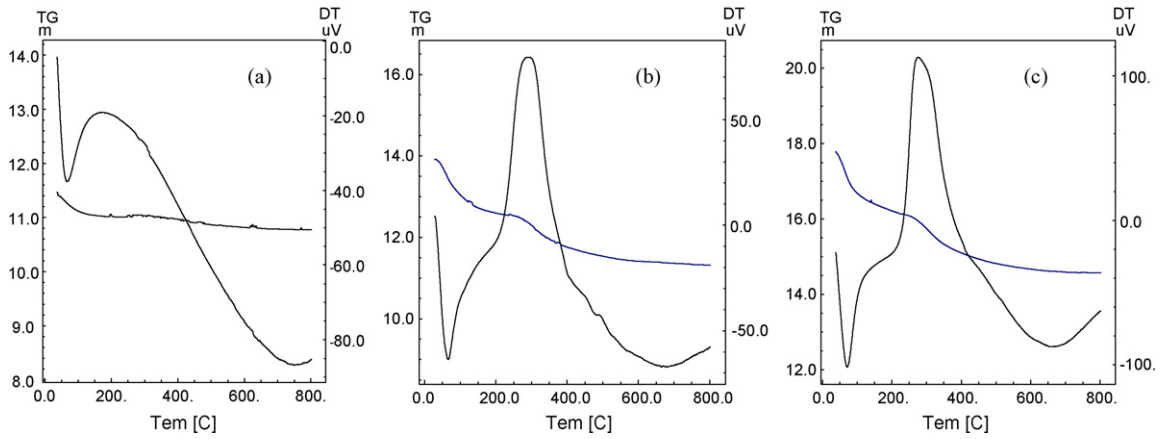

Fig. 1. DTA–TG curve for (a) SiO_2; (b) TiO_2/SiO_2 gel powder; (c) Ce-TiO_2/SiO_2 gel powder.

The size of commercial SiO_2 is in the range of 100–200 mesh. SiO_2, which was heated at 180 °C in a vacuum drying oven for 2 h, was dipped into the above sol for 30 min. After vacuum filtration, samples were transferred to an oven and cured at 60 °C, and Ce-TiO_2/SiO_2 with one Ce-doped sol–gel coating was prepared. Repeating the above process one time, a series of Ce-TiO_2/SiO_2 with two Ce-doped sol–gel coatings were obtained. The above samples calcined in air at 500 °C for 1 h, Ce-TiO_2/SiO_2 with two Ce-TiO_2 coatings were obtained. If no ammonium ceric nitrate was added, TiO_2/SiO_2 was prepared.

2.2. Characterization

The gel powders of TiO_2/SiO_2 and Ce-TiO_2/SiO_2 were subjected to thermogravimetric–differential thermal analysis (DTG-60 TG–DTA, SHIMADZU, Japan) to determine the temperature of possible decomposition and phase change. Morphology and particle size of TiO_2/SiO_2 and Ce-TiO_2/SiO_2 were determined by scanning electron microscopy (SEM) using a SEMS, Model FEI-XL30, Philips, Holand. The X-ray diffraction (XRD) patterns were obtained at room temperature with a D/Max-IIIA diffractometer ($\lambda = 0.15418$ nm). The XP spectra were collected by a VG ESCALAB MKII with a pass energy of 20 eV, and the excitation of the spectra was performed by means of monochromatized Al Kα radiation. The binding energy (BE) scale was referenced to the energy of the C 1 s peak of adventitious carbon, $E_B = 285.0$ eV. Diffuse reflectance spectra in the 200–800 nm were obtained by using a Shimadzu UV-2501PC UV–vis spectrophotometer. Reflectance spectra were referenced to $BaSO_4$.

2.2.1. Photocatalytic activity tests

Aqueous slurries were prepared by adding 0.50 g TiO_2/SiO_2 or Ce-TiO_2/SiO_2 to 400 mL-solution containing formaldehyde at 5 ppm. Irradiations were performed with a 250 W high-pressure mercury lamp. The aqueous slurries were stirred and bubbled with humid oxygen for 20 min prior to the irradiation. At 10 min intervals, the dispersion was extracted and centrifuged to separate the photocatalyst particles. The concentration of formaldehyde was analyzed by the acetylacetone spectrophotometric method [10]. This method is based on the reaction between formaldehyde, acetylacetone, and ammonium ion, which forms yellow lutidine derivate, which was measured photometrically at 414 nm. All experiments were performed at room temperature and at natural pH (pH 6.78).

3. Results and discussions

3.1. Thermal analysis

Fig. 1 shows the DTA and TGA thermodiagrams for the pure SiO_2, TiO_2/SiO_2 and Ce-TiO_2/SiO_2 nanoparticles. It can be seen from Fig. 1a that the weight of SiO_2 sharply decreases up to 70 °C and no significant weight lost was recorded from 70 to 800 °C. DTA analysis also shows that the endothermic peak at 70 °C is due to free adsorbed water. Fig. 1b shows the DTA and TGA thermodiagrams for TiO_2/SiO_2 gel powder. From the TGA analysis, the weight of TiO_2/SiO_2 sharply decreased up to 355 °C, and slowly decreased from 355 to 800 °C. DTA analysis of TiO_2/SiO_2 also shows the endothermic peak at 70 °C and exothermic peak at 290 °C. It is thought that the peak at 70 °C is due to free adsorbed water, and the peak at 290 °C is due to the decomposition of organics and at the same time corresponds to the crystallization of the amorphous phase into the anatase phase. Above 375 °C, it can be assumed that the product completely transforms into the anatase phase because there is no change in particle weight. No significant thermal effects of the transformation of the anatase phase into the rutile phase were detected even up to 800 °C.

Fig. 1c shows that the DTA and TGA curve of Ce-TiO_2/SiO_2 gel powder is similar to that of TiO_2/SiO_2. The TGA analysis shows that the weight of Ce-TiO_2/SiO_2 sharply decreases up to 345 °C, and slowly decreases from 345 to 800 °C. From the DTA analysis, a prominent endothermic peak at 70 °C is due to free adsorbed water and a exothermic peak at about 290 °C corresponds to the decomposition of organics and at the same time corresponds to the crystallization of the amorphous phase into the anatase phase. Above 380 °C, it can be assumed that the product completely transforms into the anatase phase because there is no change in particle weight. The temperature decrease of

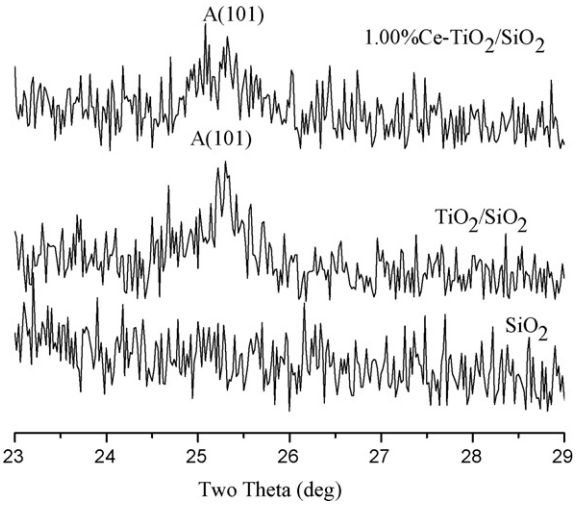

Fig. 2. XRD spectra of TiO_2, TiO_2/SiO_2, and 1.00%Ce-TiO_2/SiO_2.

this completely crystallization of the amorphous phase into the anatase phase might indicate that the cerium doping inhibits the TiO_2 phase transformation from amorphous structure to anatase.

3.2. XRD analysis

X-ray diffraction patterns of TiO_2, TiO_2/SiO_2 and 1.00%Ce-TiO_2/SiO_2 are shown in Fig. 2. The X-ray diffraction peak at 25.5° corresponds to characteristic peak of crystal plane (1 0 1) of anatase, and the peak at 27.6° corresponds to characteristic peak of crystal plane (1 1 0) of rutile. The XRD patterns of TiO_2/SiO_2 and 1.00%Ce-TiO_2/SiO_2 calcined at 500 °C shows only anatase peak. The XRD pattern of 1.00%Ce-TiO_2/SiO_2 indicates that no characteristic peaks of cerium species is found because of a low cerium dosage.

3.3. SEM analysis

Fig. 3 shows SEM photographs of these photocatalysts. Fig. 3a shows that the surface of commercial SiO_2 is slick, and some nanometer particles adhere to its surface. Fig. 3b and c shows SEM photographs of TiO_2/SiO_2 and Ce-TiO_2/SiO_2, respectively. A layer of TiO_2 or Ce-TiO_2 is obvious on the surface of SiO_2. There are some cracks on surface of some TiO_2/SiO_2 and Ce-TiO_2/SiO_2, it maybe due to the sample shrinkage caused by the crystallization of the amorphous phase into the anatase phase during calcination.

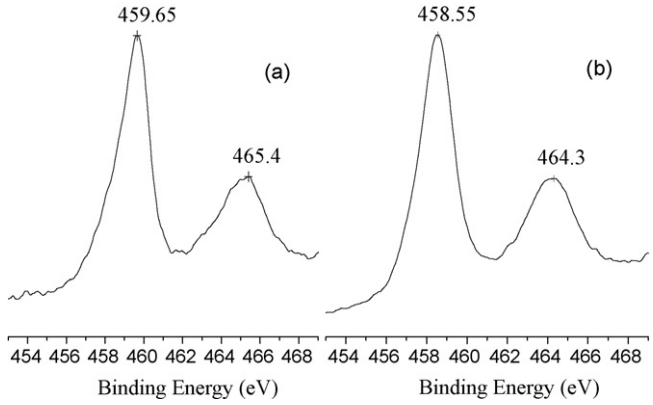

Fig. 4. Ti 2p XP spectrum for (a) TiO_2/SiO_2; (b) 1.00%Ce-TiO_2/SiO_2.

3.4. XPS analysis

Fig. 4 shows XP spectrum of Ti 2p in TiO_2/SiO_2 and 1.00%Ce-TiO_2/SiO_2. XP spectrum of Ti 2p in TiO_2/SiO_2 shows that the spin–orbit components ($2p_{3/2}$ and $2p_{1/2}$) of the peak are well deconvoluted by two curves (at 459.65 and 465.4 eV, respectively), indicating that the Ti element is present mainly as the chemical state of Ti^{4+} on the basis of literatures [11,12]. The Ti $2p_{3/2}$ peak position of TiO_2/SiO_2 shifts up from ca. 458.5 eV (for pure TiO_2) to 459.65 eV, and the binding energy increases 1.15 eV. This shift is consistent with that in the binding energy of Ti observed in literature [13]. Because the electronegativity of Si, which is 1.8, is larger than that of Ti which is 1.5. It is suggested that SiO_2 interacts with TiO_2, and the Ti–O–Si bond forms.

It seems that the peak shape of Ti 2p spectrum in 1.00%Ce-TiO_2/SiO_2 does not changed after doping cerium. The XP spectrum indicates that the Ti element mainly exists as the chemical state of Ti^{4+}, and the fixation of Ce-TiO_2 on SiO_2 did not affect the peak position of Ti 2p (at 458.55 and 464.3 eV). Compared with the upward shift of the Ti 2p peak position of TiO_2/SiO_2, it may be that the electronegativity of Si is larger than that of Ti, and the electronegativity of Ce, which is 1.1, is smaller than that of Ti. So, even if Ti–O–Ce bond and the Ti–O–Si bond forms, the binding energy of Ti 2p could hardly change.

Fig. 5 shows the Ce 3d XP spectrum of 1.00%Ce-TiO_2/SiO_2. As based on the spectral literature [8,14–15], the Cd 3d spectrum could be assigned $3d_{3/2}$ spin-orbit states and $3d_{5/2}$ states and is complex. The Ce 3d spectrum of 1.00%Ce-TiO_2/SiO_2 sample shows that Ce exists mainly in the +4 oxidation state and a little

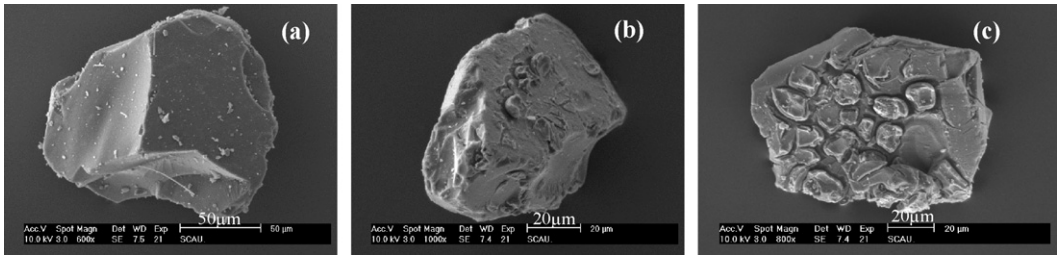

Fig. 3. SEM images of (a) SiO_2; (b) TiO_2/SiO_2; (c) 0.10%Ce-TiO_2/SiO_2.

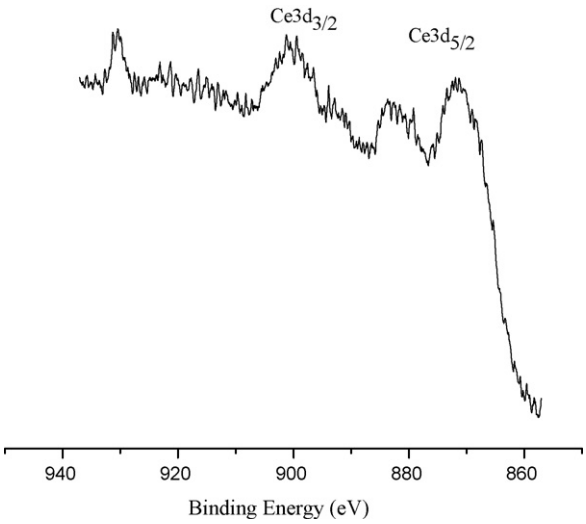

Fig. 5. Ce 3d XP spectrum of 1.00%Ce-TiO_2/ SiO_2.

in the +3 oxidation state giving rise to several peaks, indicating the coexistence of Ce^{3+} and Ce^{4+} in 1.00%Ce-TiO_2/SiO_2. So, it is indicated that cerium is present mainly in the form of CeO_2 in TiO_2. It is interesting that both Ce^{3+} and Ce^{4+} ions also resided in the cerium ion-doped catalysts even if cerium(III) nitrate was used as the dopant [8]. Because the ionic radii of Ce^{4+} and Ce^{3+} are 0.101 and 0.111 nm, respectively, much larger than that of Ti^{4+} which is 0.068 nm, it is difficult for doped-cerium ions to enter into the TiO_2 lattice and substitute Ti^{4+} to form stable solid solutions. Lin and Yu [6] have found that Ce^{4+} could not enter the TiO_2 lattice. However, cerium ions tend to bond to oxygen anion on the surface of TiO_2 nanoparticles, and Ce–O–Ti bond forms at the interface between CeO_2 and TiO_2. Moreover, at the interface, titanium ions substitutes for the cerium ions in the lattice of the surrounding cerium oxide [6–8,16].

3.5. DRS analysis

Fig. 6 gives the UV–vis spectra that show the influence of cerium on the UV–vis absorption. Modification of TiO_2/SiO_2 with cerium significantly affect the absorption properties of the

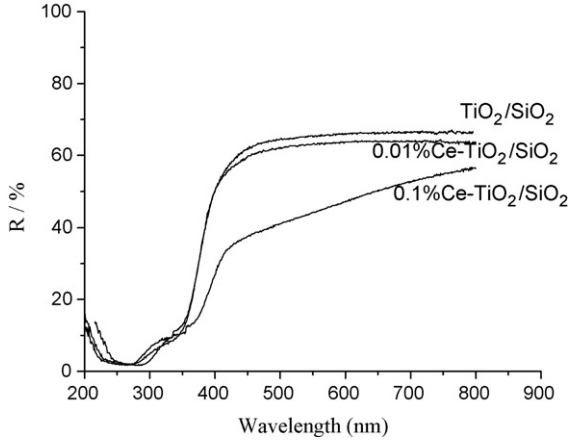

Fig. 6. DRS of Ce-TiO_2/SiO_2 with different Ce-doped content.

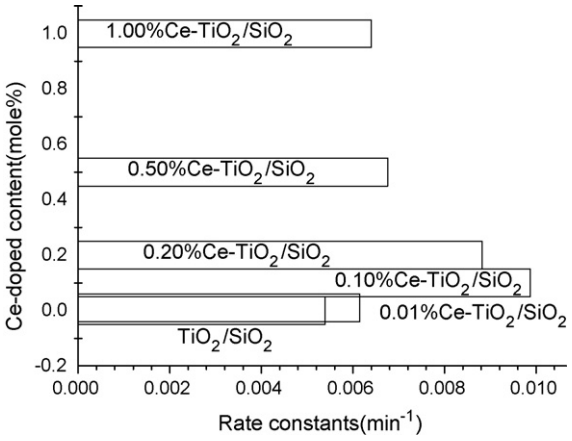

Fig. 7. Effect of the Ce-doped content on the first-order kinetics constants of TiO_2/SiO_2 for formaldehyde photocatalytic degradation.

photocatalysts. It is noticeable that a light absorption in the visible region is higher than that of TiO_2/SiO_2, and the light absorption increases with increasing cerium content. Cerium modified photocatalyst caused absorption spectra to shift to the visible region, in the range of 415–700 nm. Moreover, a larger red shift for 0.10%Ce-TiO_2/SiO_2 appears when compared to TiO_2/SiO_2. The absorption edge extends to longer wavelengths for Ce-TiO_2/SiO_2, revealing good contact between TiO_2 and Ce. For pure titania, the absorption in the ultraviolet range ($\lambda = 378$ nm) is associated with the excitation of the O 2p electron to the Ti 3d level. It is thought that the red shift is caused by the new energy level in the bandgap. Red shifts of Ce-TiO_2/SiO_2 can be attributed to the charge transfer between the TiO_2 valence or conduction band and the cerium ion 4f level [17]. As a result, the Ce-doped powders have trapping level which decreases the TiO_2 bandgap, and the Ce in the doped photocatalysts increases the visible-light absorption ability of the photocatalysts.

3.6. Effect of Ce-doped content on the photocatalytic activity of Ce-TiO_2/SiO_2

Fig. 7 shows the first-order kinetics constants of formaldehyde photocatalytic degradation over Ce-TiO_2/SiO_2 with different Ce-doped content. It is showed that the photocatalytic activity of TiO_2/SiO_2 enhanced after cerium doping, and the optimum content of cerium is 0.10 mol%. It is thought that Ce^{4+} traps easily the photo-excited electron, because Ce^{4+} ion, as a Lewis acid, apparently is superior to the oxygen molecule (O_2) in the capability of trapping electrons [7,18]. The electrons trapped in Ce^{4+} sites are subsequently transferred to the surrounding adsorbed O_2 by oxidation process. The presence of Ce on TiO_2/SiO_2 influences the photoreactivity by altering the electron–hole pair recombination rate through the following process [7]:

$$\text{electrontrapping} \quad Ce^{4+} + e^- \rightarrow Ce^{3+}$$

$$Ce^{3+} + O_2 \rightarrow {}^{\bullet}O_2^- + Ce^{4+}$$

Thus, it can be seen that the Ce 4f level in Ce-TiO_2/SiO_2 plays an important role in interfacial charge transfer and inhi-

bition of electron–hole recombination. However, it becomes the recombination center of electron–hole pair, when doping cerium content increases. Consequently it is understandable that there is an optimum value of cerium. Moreover, the incorporation of Si in a Ti-rich matrix generates a positive charge difference and the impurity cation (Si) acts as a Lewis site. It is proposed that this positive charge is balanced by hydroxyl groups, thus generating Brønsted acidity [19]. Hydroxyl groups trap hole, generating highly reactive hydroxyl radicals, and thus enhance the photocatalytic activity. So the photogenerated electron and hole are effectively separated. The UV–vis spectra show that cerium doping improves photoutilization of TiO_2, and generating more electron–hole pairs under light irradiation, which helps to improve the photocatalytic activity of TiO_2/SiO_2. At the same time, rare-earth elements have the ability of oxygen storage; they release oxygen to the system when the concentration of oxygen in the system is low, whereas they can store oxygen [20]. It is known from the photocatalytic mechanism that oxygen adsorbed on photocatalyst can trap effectively the photogenerated electron [21], so the simple recombination between electron and hole is inhibited. The redox probability increases, and the photocatalytic activity enhances.

4. Conclusions

The photocatalytic activity of TiO_2/SiO_2 enhances after cerium doping, and 0.10%Ce-TiO_2/SiO_2 exhibited optimum photocatalytic activity for formaldehyde photocatalytic degradation. The light absorption increases with increasing cerium content, and cerium doping causes absorption spectra of Ce-TiO_2/SiO_2 to shift to the visible region. Ce^{4+} traps easily the photo-excited electron, and the incorporation of Si in a Ti-rich matrix generates a positive charge that is balanced by hydroxyl groups. Hydroxyl groups trap hole, so the simple recombination of the electron–hole pair is inhibited, and thus enhancing the photocatalytic activity of Ce-TiO_2/SiO_2.

Acknowledgements

The authors would like to thank Guangdong Science & Technology Development Foundation (2007B030103019) and South China Agricultural University (2006X017) for financial supports to this work.

References

[1] A. Rachel, M. Subrahmanyam, P. Boule, Appl. Catal. B 37 (2002) 301.
[2] M. Bideau, B. Claudel, C. Dubien, L. Faure, H. Kazouan, J. Photochem. Photobiol. A 91 (1995) 137.
[3] S. Horikoshi, N. Watanabe, H. Onishi, H. Hidaka, N. Serpone, Appl. Catal. B 37 (2002) 117.
[4] S. Gelover, P. Mondragón, A. Jiménez, J. Photochem. Photobiol. A 165 (2004) 24.
[5] B. Liu, X. Zhao, N. Zhang, Q. Zhao, X. He, J. Feng, Surf. Sci. 595 (2005) 203.
[6] J. Lin, J.C. Yu, J. Photochem. Photobiol. A 116 (1998) 63.
[7] Y. Xie, C. Yuan, Appl. Catal. B 46 (2003) 251.
[8] Z.L. Liu, B. Guo, L. Hong, H. Jiang, J. Phys. Chem. Solids 66 (2005) 161.
[9] X. Yan, K. Song, M. Huo, X. Li, J. Wang, Chin. J. Appl. Chem. 16 (1999) 94.
[10] National Environmental Pretection ageacy bureau 'Analytical Methods for the Examination of Water and Wastewater' editorial board, Analytical Methods for the Examination of Water and Wastewater, Chinese Environmental Science Publishing Company, Beijing, 1998, pp. 413–416.
[11] I. Losito, A. Amorisco, F. Palmisano, P.G. Zambonin, Appl. Surf. Sci. 240 (2005) 180.
[12] J. Biener, M. Baumer, J. Wang, R.J. Madrix, Surf. Sci. 450 (2000) 12.
[13] S.M. Jung, O. Dupont, P. Grange, Appl. Catal. A 208 (2001) 393.
[14] L.S. Kastenb, J.T. Grantb, N. Grebaschc, N. Voevodin, F.E. Arnold, M.S. Donley, Surf. Coat. Technol. 140 (2001) 11.
[15] B.R. Reddy, A. Khan, Y. Yamada, T. Kobayashi, S. Loridant, J. Volta, J. Phys. Chem. B 107 (2003) 5162.
[16] H. Yang, M. Ma, X. Liu, M. Ji, J. Zhu, J. Wu, Chin. J. Chem. Phys. 10 (1997) 225.
[17] A.W. Xu, Y. Gao, H.Q. Liu, J. Catal. 207 (2002) 151.
[18] J.M. Coronado, A.J. Maira, A. Martínez-Arias, J.C. Conesa, J. Soria, J. Photochem. Photobiol. A 150 (2002) 213.
[19] N. Economidis, R.F. Coil, P.G. Smirniotis, Catal. Today 40 (1998) 27.
[20] T. Yamada, K. Kayano, M. Funabiki, Stud. Surf. Sci. Catal. 77 (1993) 329.
[21] H. Gerischer, A. Heller, J. Phys. Chem. 95 (1991) 5261.